NASA/TM—2019-220394 AIAA–2019–3895

Completion of the Long Duration Wear Test of the NASA HERMeS Hall Thruster

Jason D. Frieman, Hani Kamhawi, Jonathan A. Mackey,
Thomas W. Haag, Peter Y. Peterson, and Daniel A. Herman
Glenn Research Center, Cleveland, Ohio

James H. Gilland
Ohio Aerospace Institute, Brook Park, Ohio

Richard R. Hofer
Jet Propulsion Laboratory, Pasadena, California

December 2019

NASA STI Program . . . in Profile

Since its founding, NASA has been dedicated to the advancement of aeronautics and space science. The NASA Scientific and Technical Information (STI) Program plays a key part in helping NASA maintain this important role.

The NASA STI Program operates under the auspices of the Agency Chief Information Officer. It collects, organizes, provides for archiving, and disseminates NASA's STI. The NASA STI Program provides access to the NASA Technical Report Server—Registered (NTRS Reg) and NASA Technical Report Server—Public (NTRS) thus providing one of the largest collections of aeronautical and space science STI in the world. Results are published in both non-NASA channels and by NASA in the NASA STI Report Series, which includes the following report types:

- TECHNICAL PUBLICATION. Reports of completed research or a major significant phase of research that present the results of NASA programs and include extensive data or theoretical analysis. Includes compilations of significant scientific and technical data and information deemed to be of continuing reference value. NASA counter-part of peer-reviewed formal professional papers, but has less stringent limitations on manuscript length and extent of graphic presentations.

- TECHNICAL MEMORANDUM. Scientific and technical findings that are preliminary or of specialized interest, e.g., "quick-release" reports, working papers, and bibliographies that contain minimal annotation. Does not contain extensive analysis.

- CONTRACTOR REPORT. Scientific and technical findings by NASA-sponsored contractors and grantees.

- CONFERENCE PUBLICATION. Collected papers from scientific and technical conferences, symposia, seminars, or other meetings sponsored or co-sponsored by NASA.

- SPECIAL PUBLICATION. Scientific, technical, or historical information from NASA programs, projects, and missions, often concerned with subjects having substantial public interest.

- TECHNICAL TRANSLATION. English-language translations of foreign scientific and technical material pertinent to NASA's mission.

For more information about the NASA STI program, see the following:

- Access the NASA STI program home page at http://www.sti.nasa.gov

- E-mail your question to help@sti.nasa.gov

- Fax your question to the NASA STI Information Desk at 757-864-6500

- Telephone the NASA STI Information Desk at 757-864-9658

- Write to:
  NASA STI Program
  Mail Stop 148
  NASA Langley Research Center
  Hampton, VA 23681-2199

NASA/TM—2019-220394 AIAA–2019–3895

Completion of the Long Duration Wear Test of the NASA HERMeS Hall Thruster

Jason D. Frieman, Hani Kamhawi, Jonathan A. Mackey,
Thomas W. Haag, Peter Y. Peterson, and Daniel A. Herman
Glenn Research Center, Cleveland, Ohio

James H. Gilland
Ohio Aerospace Institute, Brook Park, Ohio

Richard R. Hofer
Jet Propulsion Laboratory, Pasadena, California

Prepared for the
Propulsion and Energy Forum and Exposition
sponsored by the American Institute of Aeronautics and Astronautics
Indianapolis, Indiana, August 19–22, 2019

National Aeronautics and
Space Administration

Glenn Research Center
Cleveland, Ohio 44135

December 2019

Acknowledgments

The authors would like to thank Drew Ahern, Maria Choi, Thomas Haag, Wensheng Huang, Jon Mackey, Luis Pinero, Timothy Sarver-Verhey, George Williams, and John Yim also of the Electric Propulsion Systems Branch at NASA Glenn Research Center (GRC) for their contributions to the overall success of the Long Duration Wear Test (LDWT). The authors would also like to thank Scott Hall, Dale Robinson, and Jim Myers of Vantage Partners, LLC for their work, technical input, and guidance as well as Taylor Varouh, Chad Joppeck, Kevin Blake, George Jacynycz, Roland Gregg, Josh Gibson, Matt Daugherty, James Szelagowski, James Zakany, and all of the engineers, technicians, and managers of the Space Environments Test Branch (FTF) for the fabrication, assembly of the test setup, and operation of the vacuum facility. Finally, the authors would like to thank Jet Propulsion Laboratory (JPL) team members Ioannis Mikellides, Vernon Chaplin, Robert Lobbia, Alejandro Lopez-Ortega, and James Polk.

Level of Review: This material has been technically reviewed by technical management.

Available from

NASA STI Program
Mail Stop 148
NASA Langley Research Center
Hampton, VA 23681-2199

National Technical Information Service
5285 Port Royal Road
Springfield, VA 22161
703-605-6000

This report is available in electronic form at http://www.sti.nasa.gov/ and http://ntrs.nasa.gov/

Completion of the Long Duration Wear Test of the NASA HERMeS Hall Thruster

Jason D. Frieman, Hani Kamhawi, Jonathan A. Mackey, Thomas W. Haag,
Peter Y. Peterson, and Daniel A. Herman
National Aeronautics and Space Administration
Glenn Research Center
Cleveland, Ohio 44135

James H. Gilland
Ohio Aerospace Institute
Brook Park, Ohio 44142

Richard R. Hofer
Jet Propulsion Laboratory
Pasadena, California 91109

Abstract

The NASA Hall Effect Rocket with Magnetic Shielding (HERMeS) 12.5-kW Hall thruster has been the subject of extensive technology maturation by NASA Glenn Research Center (GRC) and Jet Propulsion Laboratory (JPL) in preparation for development into a flight propulsion system. As part of this effort, a series of wear tests have been conducted to identify erosion phenomena and the accompanying failure modes as well as to validate service-life models for magnetically-shielded thrusters. This work presents a summary of the results obtained during the Long Duration Wear Test (LDWT), which was the third in this wear test series. The LDWT accumulated approximately 3,570 hours of operation and had the overall goal to identify and correct design or facility issues prior to the flight qualification campaign. Thruster performance, stability, and plume properties were invariant throughout the duration of the LDWT and consistent with measurements acquired during previous HERMeS performance and wear characterizations. Average erosion rates of a carbon-carbon composite pole cover were found to match those measured with graphite to within the empirical uncertainty while the previously observed time-dependence of pole cover erosion rates was linked to changes in pole cover roughness. Azimuthal variations in keeper wear rate were observed including deposition on one of the azimuthal-facing sides of the keeper mask. This strongly suggests the presence of an azimuthal component in the process driving keeper erosion.

1.0 Introduction

NASA continues to evolve a human exploration approach for beyond low Earth orbit and to do so, where practical, in a manner involving international, academic, and industry partners (Ref. 1). This approach is based on an evolutionary human exploration architecture beginning with the establishment of a Gateway around the Moon to enable long-term lunar exploration and utilization followed by crewed missions beyond the Earth-moon system.

High-power solar electric propulsion (SEP) is one of those key technologies that has been prioritized because of its significant exploration benefits. Specifically, for missions beyond low Earth orbit, spacecraft size and mass can be dominated by onboard chemical propulsion systems and propellants that may constitute more than 50 percent of spacecraft mass. This impact can be significantly reduced through

the utilization of SEP due to its substantially higher specific impulse. Studies performed for NASA's Human Exploration and Operations Mission Directorate and Science Mission Directorate have demonstrated that a 40-kW-class SEP capability can be enabling for both near term and future architectures and science missions (Ref. 2). In addition, a high-power, 40-kW-class Hall thruster propulsion system provides significant capability and represents, along with flexible blanket solar array technology, a readily scalable technology with a clear path to much higher power systems.

Accordingly, since 2012, NASA has been developing a high-power Hall thruster electric propulsion string that can serve as the building block for realizing a 40-kW-class SEP capability. The Hall thruster system development, led by the NASA Glenn Research Center (GRC) and the Jet Propulsion Laboratory (JPL), began with maturation of the 12.5-kW Hall Effect Rocket with Magnetic Shielding (HERMeS) and power processing unit. The technology development work has since transitioned to Aerojet Rocketdyne via a competitive procurement selection for the Advanced Electric Propulsion System (AEPS) contract, which includes the further development and qualification of electric propulsion strings. The AEPS Electric Propulsion string consists of the 12.5-kW Hall thruster, power processing unit (including digital control and interface functionality), xenon flow controller, and associated intra-string harnesses. NASA continues to support the AEPS development by leveraging in-house expertise, plasma modeling capability, and world-class test facilities. NASA also executes AEPS and mission risk reduction activities to support the AEPS development and mission application.

As part of this effort, NASA has conducted a series of three wear tests to identify erosion phenomena and the accompanying failure modes as well as to validate service-life models for magnetically-shielded thrusters. These tests utilized two different technology demonstration unit (TDU) thrusters with similar designs. The first began in 2016 and accumulated approximately 1,700 hours of operation using the TDU-1 thruster (Ref. 3). The second was performed in 2017 with the TDU-3 thruster and consisted of a series of seven short duration (~200 h) segments each testing a different thruster configuration or operating condition (Ref. 4). This test is referred to as the TDU-3 Short Duration Wear Test (SDWT) throughout this paper.

This work presents an overview and summary of the results obtained from the third wear test (named the TDU-3 Long Duration Wear Test or TDU-3 LDWT), which began in October 2017 and was completed in October 2018. The overall goal of this test was to quantify performance, stability, plume, and wear trends of TDU-3 over at least 3,000 hours of operation. In addition to providing additional data to assist in the identification, quantification, and modeling of erosion phenomena, the TDU-3 LDWT served as a pathfinder for the planned life and qualification testing of the hardware to be delivered as part of the AEPS contract as well as two novel diagnostics: a thrust vector probe (TVP) and in-situ wear tool (Refs. 5 and 6). Overall, the TDU-3 LDWT provided NASA the opportunity to develop the experience and procedures for operating high-power long duration testing, thus lowering the risks for all future extended duration tests.

2.0 Test Segment Summary

The TDU-3 LDWT accumulated approximately 3,570 hours of total operating time split between six wear segments. A summary of these segments is shown in Table 1.

Segment I was performed at the nominal TDU operating condition of 600 V/12.5 kW and resulted in the accumulation of 1015 hours of operating time. This segment was interrupted by a facility anomaly and so was completed in two consecutive parts lasting 620 and 395 h, respectively. The elevated facility pressure measured during this segment was most likely due to initial outgassing and bake out of the carbon panels lining the facility walls. This is supported by the fact that the facility operating pressure was observed to decrease from approximately 8 to 4 μTorr over the course of this segment.

TABLE 1.—TDU-3 LDWT TEST SEGMENTS

Segment	I	II	III	IV	V	VI
Operating condition[a]	600 V/1 B	300 V/1 B	300 V/0.75 B	300 V/1.25 B	600 V/1 B	600 V/1 B
Facility pressure, μTorr	5.7	4.2	4.1	4.2	4.3	11.7
Segment duration, h	1015	252	214	240	1579	270

[a]All segments completed at a discharge current of approximately 20.8 A.

Segments II-IV were all performed at the 300 V/6.25 kW throttle point, however, each was performed at a different magnetic field strength. Segment II was performed at the nominal magnetic field strength (1 B) while Segments III and IV were performed at field strengths of 0.75 B and 1.25 B. Each of these segments lasted for between 200 and 250 h and has been detailed in previous work (Ref. 7).

Segment V was performed at the nominal TDU operating condition of 600 V/12.5 kW and resulted in the accumulation of 1579 hours of operating time with a carbon-carbon (C-C) composite inner front pole cover (IFPC). This was done in order to assess the lifetime of an alternate pole cover material with increased strength and crack resistance. This segment was interrupted by three anomalies and so was completed in four consecutive parts lasting approximately 555, 241, 380, and 403 h, respectively. Segment VI was also performed at the 600 V/12.5 kW operating condition. However, unlike Segments I and V, Segment VI was performed at an elevated facility pressure of approximately 11.7 μTorr in order to assess the impact of facility background pressure on HERMeS wear rates.

3.0 Experimental Apparatus

3.1 HERMeS TDU-3

All wear segments were performed using the 12.5-kW NASA HERMeS TDU-3. The overall HERMeS design incorporates technologies developed by NASA over nearly two decades, including a magnetic shielding topology to eliminate discharge channel erosion as a life-limiting mechanism. The result is a significant increase in the operational lifetime of state-of-the-art Hall Effect Thrusters (HETs), with HERMeS being designed to operate at a specific impulse of 3,000 s for an operational lifetime exceeding 50 kh (Refs. 8 to 12).

The HERMeS TDU-3 thruster is shown in the configuration used for the majority of the LDWT in Figure 1. The thruster configuration was largely unchanged from that used during the previous TDU-3 SDWT, with two exceptions (Ref. 4). First, a pair of new magnet coils were installed in TDU-3 prior to the LDWT. This resulted in a change in the current settings required to achieve a fixed magnetic field strength, but did not change the magnetic field shape.

The second exception was the position and thickness of the cathode keeper. During the TDU-1 wear test, the cathode keeper was positioned upstream of the IFPC, and negligible keeper erosion was observed (Refs. 3 and 4). During the TDU-3 SDWT, changes to the design of the IFPC resulted in a keeper position that was coplanar with the downstream surface of the IFPC; this represents a downstream shift relative to the TDU-1 position by a distance approximately equal to the thickness of the IFPC (Ref. 4). Despite the small positional shift, results from the SDWT indicated average keeper erosion rates of approximately 80 μm/kh at the same operating condition used for the TDU-1 wear test; these rates were the largest observed for any thruster component during the SDWT (Ref. 4). For the TDU-3 LDWT, the cathode was returned to the position used during the TDU-1 wear test (i.e., upstream of the IFPC), in order to investigate this as an approach for mitigating the elevated keeper wear observed during the SDWT (Refs. 4 and 7). In addition, the keeper thickness was doubled during the LDWT to provide added lifetime margin. The impacts of these keeper changes are discussed in previous work (Ref. 7). The same cathode (here defined as heater, tube, and insert) was used for all 3 TDU wear tests.

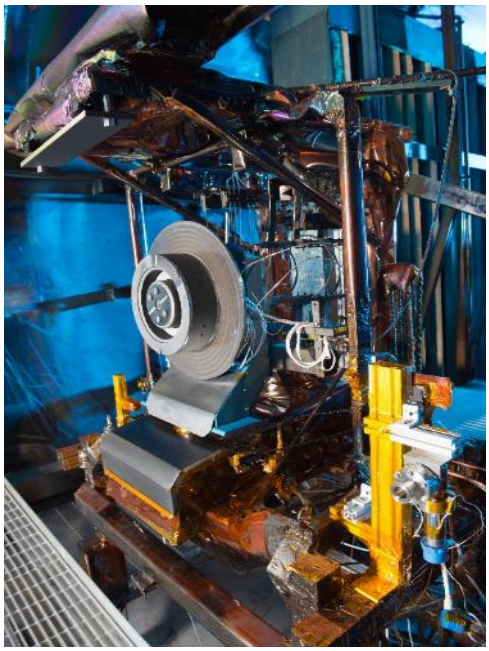

Figure 1.—HERMeS TDU-3 Hall thruster in the configuration used for the LDWT.

Although the cathode position used during the LDWT matches that used during the TDU-1 wear test, a number of other small design changes differentiate TDU-3 and TDU-1 including a change in the grade of boron nitride used for the discharge channel. A detailed description of these changes is provided in Kamhawi et al. (Ref. 9); the results from that work suggest they resulted in minimal changes to HET performance, stability, and plume properties.

3.2 Thruster Support Equipment

Xenon propellant was supplied to the thruster and the centrally-mounted cathode using a laboratory feed system composed of stainless-steel lines metered with commercial thermal mass flow controllers. The anode line was metered using a 500-sccm controller, and the cathode line was metered using a 100-sccm controller. All controllers were calibrated before Segments I and V and after Segment VI using a NIST-traceable piston prover. The controllers had a measured uncertainty of approximately 1 sccm for the anode and 0.2 sccm for the cathode (Ref. 13). This system was identical to that used in previous TDU wear tests (Refs. 3 and 4).

All power to TDU-3 was provided using a power console composed of commercial laboratory power supplies. The discharge was controlled using three 15-kW (1000 V, 15 A) power supplies connected in a master-slave configuration. The output from these supplies was connected to a laboratory wire harness with an inductance and capacitance of approximately 2.5 μH and 236 pF, respectively (Ref. 14). This console was equipped with a set of safety interlocks that allows the data acquisition or vacuum facility control system to disable power and place the thruster in a safe state in the event that a facility or thruster anomaly is detected. This setup was unchanged from previous HERMeS characterization and wear tests (Refs. 3, 4, 9, 15 to 17).

Following the results from the electrical configuration study performed by Peterson et al. (Ref. 17), the TDU-3 thruster body was electrically tied to the cathode, and all conductive surfaces within approximately 1 m of the thruster exit plane were insulated using dielectric sheeting (Refs. 17 and 18). This was done in order to provide better control over the number of electrical coupling paths between the HET and facility in the near-field (Refs. 17 and 18).

Thruster telemetry was recorded continuously at a rate of approximately 0.5 Hz using a multiplexed data acquisition system. End-to-end calibrations of the laboratory power and data acquisition systems (DAQ) were performed before and after the test using a NIST-traceable digital multimeter. The resultant uncertainty was approximately ±0.06 V and ±0.03 A for measurements of voltage and current, respectively. Nearly all voltages were measured both at the breakout box (BoB) and via a sense line at the interface between TDU-3 and the facility cable harness. Unless otherwise noted, all voltages reported in this work correspond to the measurements from the sense lines.

Three oscilloscopes were used to monitor oscillations during the LDWT. The first two oscilloscopes were used to compute the root-mean-square (RMS) and peak-to-peak values of the discharge current, discharge voltage, cathode-to-ground voltage, keeper voltage, and body voltage. These measurements were obtained over intervals of 100,000 samples at a sampling rate of 1 MS/s and recorded by the DAQ. The final oscilloscope was used to obtain waveforms of the AC components of the discharge current, discharge voltage, and keeper voltage. These waveforms consisted of 5 million points sampled at a rate of 50 MS/s. All oscillation data reported in this work were collected using this third oscilloscope. For all three oscilloscopes, current measurements were acquired using 150-A AC/DC current probes while voltage measurements were acquired using high-voltage differential probes.

3.3 Vacuum Facility

All experiments detailed in this work were performed in VF-5 at NASA GRC. VF-5 is a cylindrical chamber measuring 4.6 m in diameter and 18.3 m in length (Ref. 19). For this test, VF-5 was evacuated using a series of cryopumps. The cryopumps have a total effective pumping area of 33.5 m^2 and a combined nominal pumping speed of approximately 700,000 l/s on xenon (Refs. 19 to 21). In order to obtain the lowest possible background pressure, the thruster was installed in the main volume of VF-5 at the same location previously used during the TDU-1 wear test and the TDU-3 SDWT (Refs. 3 and 4). The placement of the cryopumps relative to the thruster at this location as well as the resultant near-field background neutral distribution are described in previous work (Refs. 19 to 21).

As shown in Figure 2, facility pressure was monitored with two xenon-calibrated and one nitrogen-calibrated Bayard-Alpert style hot-cathode ionization gauges. One xenon-calibrated gauge (SIG 3 Xe) was centered approximately 0.7 m radially outward, 0.08 m upstream, and 0.6 m below the HET exit plane. The orifice of SIG 3 Xe faced radially outward (i.e., away from the HET).

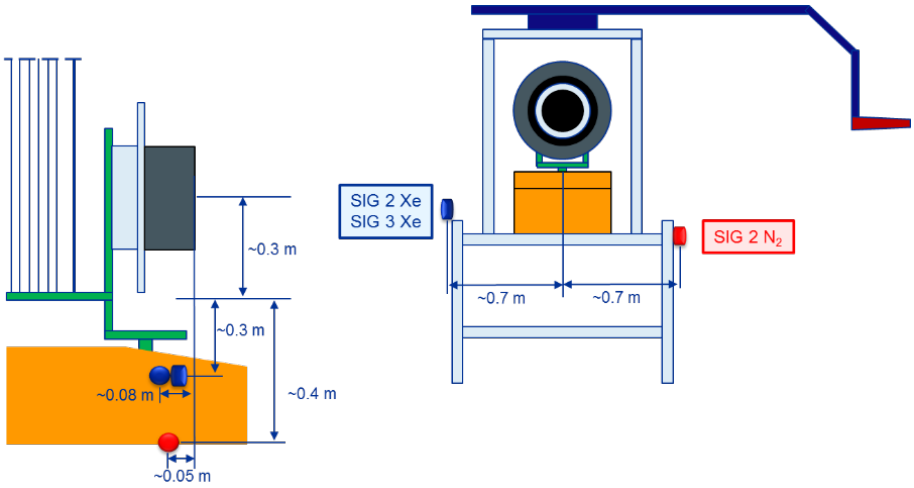

Figure 2.—Ion gauge configuration used during Segments V-VI of the TDU-3 LDWT (not to scale).

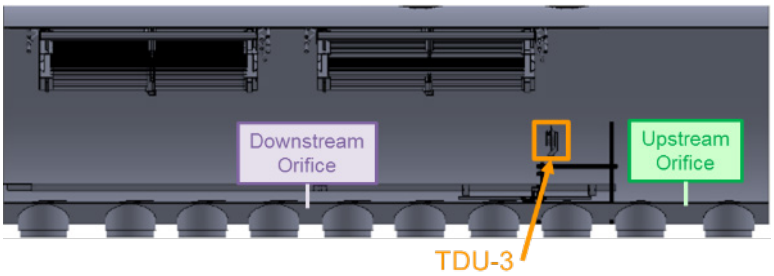

Figure 3.—Locations of bleed flow orifices used during Segment VI of the TDU-3 LDWT.

The second xenon-calibrated gauge (SIG 2 Xe) was mounted adjacent to and downstream of SIG 3 Xe and had a downstream-facing orifice. The nitrogen-calibrated gauge (SIG 2 N_2) was located approximately 0.7 m radially outward, 0.05 m upstream, and 0.4 m below the HET exit plane. The orifice of SIG 2 N_2 faced radially outward. SIG 2 Xe and SIG 2 N_2 were relocated to these positions prior to the start of Segment V in order to accommodate installation of the TVP. Details of their positions during Segments I-IV are available in Reference 7.

All ion gauges used in this work were configured for operation with electric propulsion systems and thus had an elbow and plasma screen installed on the inlet of the gauge (Ref. 22). The housing of each gauge was also attached to facility ground via an electrical grounding strap to avoid charging effects. A thermocouple was installed on the exterior of each ion gauge tube; this allowed the measured pressures to be corrected for thermal effects (Ref. 23). The gauge temperatures and pressures were sampled using the same multiplexed DAQ used to record thruster telemetry (Ref. 22). Consistent with previous tests performed in VF-5, all pressures reported in this work correspond to the measurements made using SIG 3 Xe (Refs. 3, 4, 9, 15 to 17).

In order to raise the operating pressure during Segment VI, a bleed or auxiliary flow of xenon was injected into VF-5 through a pair of orifices installed near the bottom of the facility. As shown in Figure 3, the first orifice was installed downstream of TDU-3 at approximately the mid-point of the facility. This position is identical to the one used during the TDU-1 Facility Effect Characterization Test (FECT) (Ref. 16). The second was installed between the two cryopanels located upstream of TDU-3. In order to avoid artificially introducing bulk neutral motion, both orifices were equipped with diffusers and a barrier to prevent flow injection towards the thruster (Ref. 24). During Segment VI, the bleed flow rates through each orifice were varied until the ion gauges facing radially (i.e., SIG 2 Xe) and downstream (SIG 3 Xe) both read approximately 11 μTorr. This was done in order to provide the closest analog to the near-field backpressure environment observed for TDU operation in VF-6 at NASA GRC (Ref. 25).

3.4 Diagnostics

This section discusses the heritage diagnostics used during the TDU-3 LDWT. Information regarding the new TVP and In-situ Wear Diagnostic demonstrated during the LDWT can be found in References 5 and 6, respectively.

3.4.1 Thrust Stand

Thrust was measured using the same null-type inverted pendulum thrust stand used in previous HERMeS performance characterization and wear tests (Refs. 3, 4, 9, 15 to 17). The design and theory of operation of the thrust stand are detailed in several previous works (Refs. 26 to 28).

During the LDWT, the thrust stand was operated in a null-coil configuration. In this configuration, the position of the thruster is measured by a linear variable differential transformer (LVDT) and maintained by a pair of electromagnetic actuators. The current through each actuator is controlled using an integral-differential controller that uses the LVDT signal as the input and then modulates the current through the actuators in order to hold the thruster stationary. The thrust is then correlated to the resultant current through one of these actuators (i.e., the null coil). The thrust stand is also equipped with a closed-loop inclination control circuit, which uses an integral controller and piezoelectric actuator to maintain the inclination measured by an electrolytic tilt sensor and thus minimize thermal drift during performance measurements.

The thrust stand was calibrated before each performance characterization period by loading and offloading a set of known weights using an in-situ pulley system. All reported thrust measurements have been corrected for thermal drift and offsets from the desired discharge power. The resultant thrust stand uncertainty for this work is approximately ±5 mN (Ref. 29).

3.4.2 Facility Backsputter

Measurements of facility backsputter were obtained using three quartz crystal microbalances (QCMs) (Ref. 30). As shown in Figure 4, the QCMs were located approximately 1 m radially outward from the centerline of the thruster in the thruster exit plane. All three QCMs faced downstream and were water cooled with three parallel cooling loops from a single chiller. Each QCM was also equipped with an electrically-actuated shutter in order to prevent saturation of the crystals during the wear test. The total deposited thickness was measured by the QCM controller and recorded by the same DAQ used for thruster telemetry. The measured thickness was then post-processed in order to compute the average backsputter rate using the techniques described by Gilland et al. (Ref. 30).

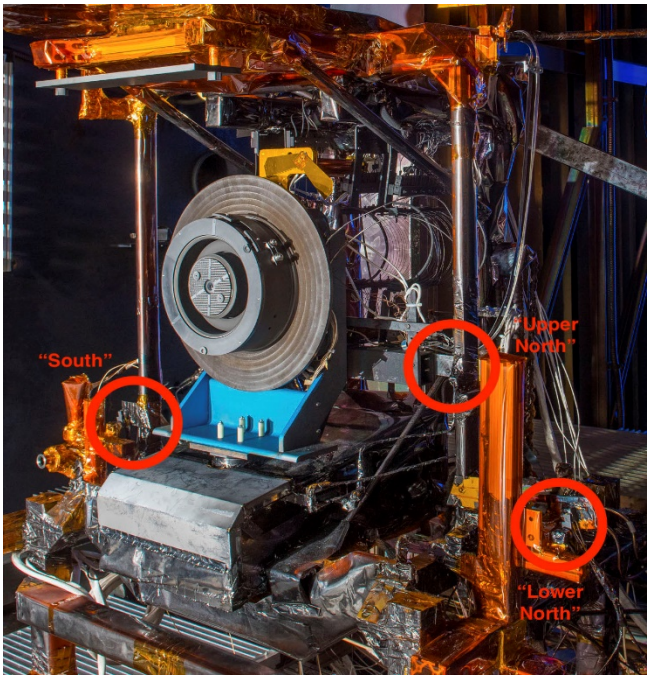

Figure 4.—QCM locations and naming convention used during the TDU-3 LDWT.

3.4.3 Plasma Diagnostics

Plume properties were measured using a Faraday probe (FP), Langmuir probe (LP), retarding potential analyzer (RPA), and a Wien filter spectrometer (WFS or ExB probe). The probes were integrated into a single array mounted to a two-axis positioning system, which controls the position of the probes in the azimuthal and radial directions relative to the thruster. These diagnostics have been used in previous HERMeS characterization and wear tests and are further detailed in Huang et al. (Ref. 16).

3.5 Erosion Measurements

3.5.1 Profilometer

All erosion measurements were made with a chromatic, white-light non-contact benchtop profilometer. The employed profilometer is equipped with an optical pen oriented normal to the HET exit plane with a 3-mm measuring range. All acquired profilometry data were analyzed according to the guidance established in the ISO 5436-1 measurement standard for a type A1 step (i.e., a wide groove with a flat bottom) (Ref. 31). Uncertainty was quantified using the technique detailed by Mackey et al. (Ref. 32) that accounts for instrument error, surface roughness, wear due to operation at points other than the nominal wear point, and the non-flat nature of the acquired profiles. The results of this uncertainty analysis yielded typical uncertainties on the order of ±2 μm for this work.

3.5.2 Wear Surface Configuration

Similar to the approach taken in previous HERMeS wear tests, the IFPC, outer front pole cover (OFPC), and keeper were modified in order to better characterize component erosion rates (Refs. 3 and 4). Specifically, graphite masks were installed to provide unexposed surfaces to use as a reference for post-test analysis. This section details the placement of these masks as well as the other features of the IFPC, OFPC, and keeper configurations used during Segments V and VI of the LDWT. Details on these surfaces for Segments I-IV are available in Reference 7.

The IFPC configuration used during Segment V of the LDWT is shown in Figure 5(a). The IFPC was made of a carbon-carbon composite instead of the graphite used for the other LDWT segments. Identical masks to those used during the other LDWT segments were installed at the 12 and 8 o'clock positions while a pair of bushings were installed at the 4 and 10 o'clock positions (Ref. 7). Similar to the approach taken with the molybdenum strips during the SDWT, two grooves were incorporated into the C-C IFPC to accommodate a pair of graphite inserts (Ref. 4). These inserts were installed in the grooves and laid flush with the downstream surface of the IFPC. In order to investigate the impact of surface finish on IFPC erosion, the insert installed at the 6 o'clock position was polished before installation whereas the one at the 2 o'clock position was not. Unfortunately, the small size of the inserts relative to the masks precluded obtaining measurements of insert wear following Segment V. The IFPC configuration used during Segment VI of the LDWT is shown in Figure 5(b). This configuration is identical to that used during Segments I-IV of the LDWT and is detailed in Reference 7.

The OFPC used during Segment V of the LDWT is shown in Figure 6(a). The OFPC was made of graphite and had the region between 7 and 10 o'clock polished pre-test. Two masks were installed at the 12 and 9 o'clock positions. These masks and OFPC configuration were identical to those used during the SDWT and previous LDWT segments (Refs. 4 and 7).

Segment VI reused the graphite OFPC from Segment IV (Ref. 7). As shown in Figure 6(b), the 3 to 4 o'clock region of this OFPC was polished pre-test. Two masks were installed over the polished region at the 3 and 4 o'clock positions. An additional mask was installed over the unpolished region of OFPC at the 10 o'clock position. It is important to note that this is the only pole cover used during the

LDWT to undergo re-polishing between test segments and that the mask at 10 o'clock was installed over a region of the pole cover that was never polished.

The keeper configuration used during the TDU-3 LDWT is shown in Figure 5(b). The keeper was made of graphite and had the downstream surface polished prior to installation. A graphite ring was affixed to the outer edge of the downstream keeper face. This ring increased the diameter of the keeper to match the AEPS design and provided a masked reference surface for keeper erosion measurements. A small tab was also included as part of the mask, which protruded radially inwards towards the cathode orifice. This tab enabled an assessment of the radial variation in erosion rates across the keeper face. A new keeper was installed prior to the start of Segment V. It was re-used for Segment VI, but the mask was rotated prior to the start of that segment to expose a new region of polished graphite. This enabled direct measurements of the keeper wear for both segments.

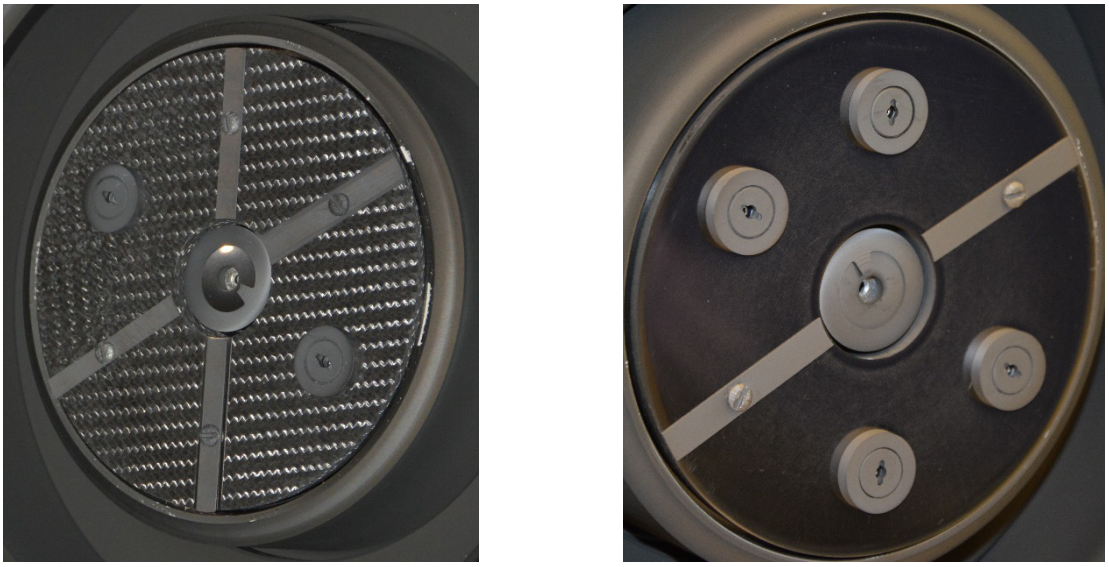

(a) (b)

Figure 5.—IFPC configurations used during Segments (a) V and (b) VI of the TDU-3 LDWT.

(a) (b)

Figure 6.—OFPC configurations used during Segments (a) V and (b) VI of the TDU-3 LDWT.

4.0 Results and Discussion

4.1 Overview

Similar to the approach taken in previous TDU wear tests, continuous operation at each of the conditions listed in Table 1 was periodically interrupted in order to acquire performance, stability, and plume data for the reference firing conditions shown in Table 2. It is important to note that, even during Segment VI, these reference firings were performed at the nominal operating pressures for VF-5. During the LDWT, these average facility pressures were approximately 3 μTorr-Xe for operation at RFC 1 and 4.5 μTorr-Xe for all other conditions.

4.2 Thrust

The thrust of TDU-3 measured at each of the RFCs from Table 2 is shown as a function of total operating time in Figure 7. The statistics of these data are shown in Table 3. The measured thrust of TDU-3 during the LDWT varied by less than the thrust stand uncertainty (±5 mN) for all RFCs. Furthermore, as shown in Table 3, these measurements differ from those obtained during the TDU-1 wear test by less than the empirical uncertainty (Refs. 3 and 4). This performance invariance is an indicator of the effectiveness of the HERMeS magnetic shielding topology as previous wear tests performed on non-magnetically shielded thrusters have observed a decrease in performance during the first 1000 h of operation (Ref. 33). This decrease in performance has been attributed to erosion of the discharge channel walls, which is a phenomenon that is minimized by magnetic shielding (Ref. 33).

TABLE 2.—REFERENCE FIRING CONDITIONS USED DURING THE TDU-3 LDWT

RFC	Discharge voltage, V	Discharge current, A	Discharge power, W
1	300	9.00	2700
2	300	20.83	6250
3	400	20.83	8333
4	500	20.83	10417
5	600	20.83	12500
6	630	20.83	13123

TABLE 3.—THRUST STATISTICS FOR TDU-3 LDWT AND TDU-1 WEAR TEST

RFC		TDU-1 wear test		TDU-3 LDWT	
		Thrust, mN	Standard deviation, mN	Thrust, mN	Standard deviation, mN
1	300 V, 2.7 kW	-------	-------	167.5	2.4
2	300 V, 6.3 kW	393.1	2.8	395.5	2.2
3	400 V, 8.3 kW	477.5	1.9	479.1	2.1
4	500 V, 10.4 kW	544.8	6.7	545.7	2.4
5	600 V, 12.5 kW	610.1	2.4	612.9	2.0
6	630 V, 13.1 kW	-------	-------	630.3	2.2

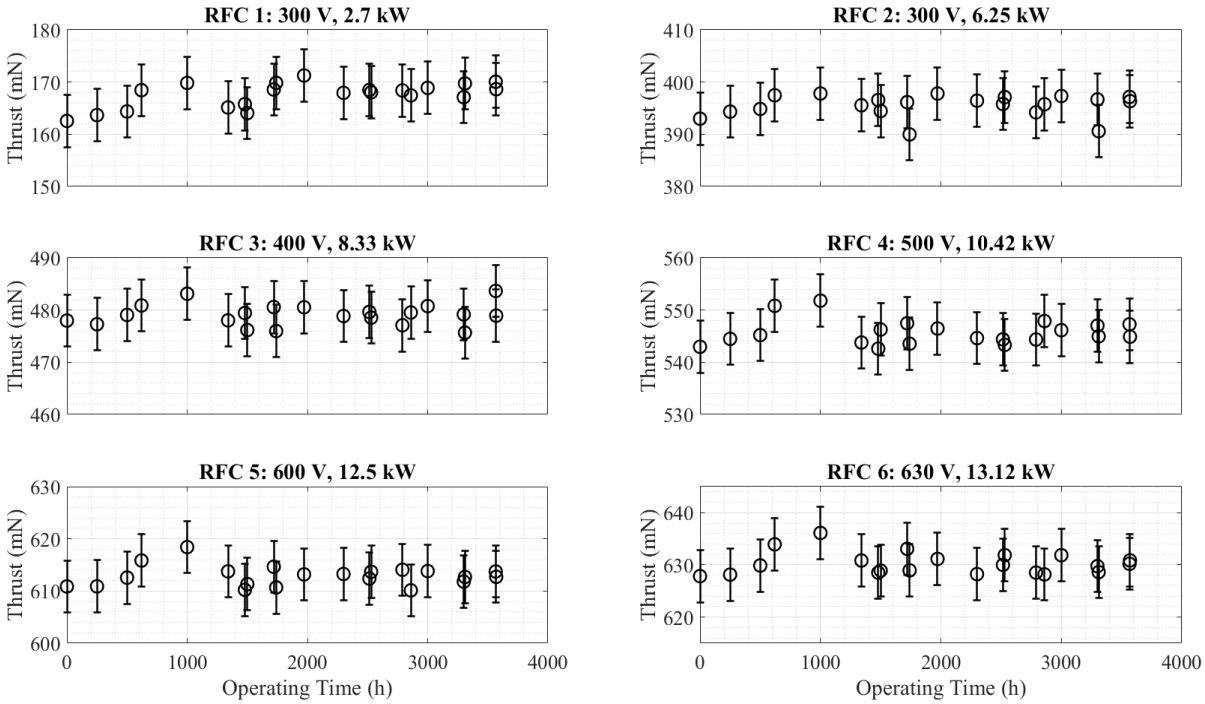

Figure 7.—TDU-3 thrust as a function of operating time during the LDWT.

4.3 Discharge Current Oscillations

The discharge current oscillations of TDU-3 were characterized using the peak-to-peak (I_{dPk2Pk}) and root-mean-square (I_{dRMS}) of the recorded current waveform. The results were normalized by the average discharge current (I_d) and are plotted as a function of operating time for each of the RFCs in Figure 8. Similar to the performance results discussed in Section 4.2, the discharge current oscillations varied by less than 4 percent for all RFCs over the LDWT. This consistency was also observed in the measured power spectral densities, which showed standard deviations of less than 2.5 kHz and 2 dB for peak frequencies and powers. The stability and spectral characteristics measured during the LDWT are consistent with those obtained during previous TDU wear and performance characterizations (Refs. 3, 4, 9, 15 to 17).

4.4 Plume Properties

Faraday probe results acquired for operation at RFC 5 (600 V/12.5 kW) during the LDWT are plotted as a function of operating time in Figure 9(a). Each plot in this section contains a line representing the mean and standard deviation (represented by the error bars) of all values obtained during the LDWT. The mean charge-weighted divergence angle was 19.7°, with a standard deviation of 0.32° (1.6 percent) while the average ion beam current was 18.9 A, with a standard deviation of 0.60 A (3.2 percent). All angles in this section are measured relative to the thruster centerline axis.

As discussed extensively in Reference 34, high-energy ions have been observed across a wide range of angular positions in the HERMeS plume. In order to characterize the divergence of these ions, previous studies have found the angle at which the high-energy peak in the RPA trace becomes undetectable relative to the noise floor of the measurement. This angle is referred to as the maximum high-energy polar angle and is shown in Figure 9(b). RPA measurements were taken in 5° intervals in the wings of the plume. The resultant ±2.5° resolution is represented by the error bars in Figure 9(b). The mean high-energy polar angle over the LDWT was 71.9°, with a standard deviation of 2.9° (4 percent).

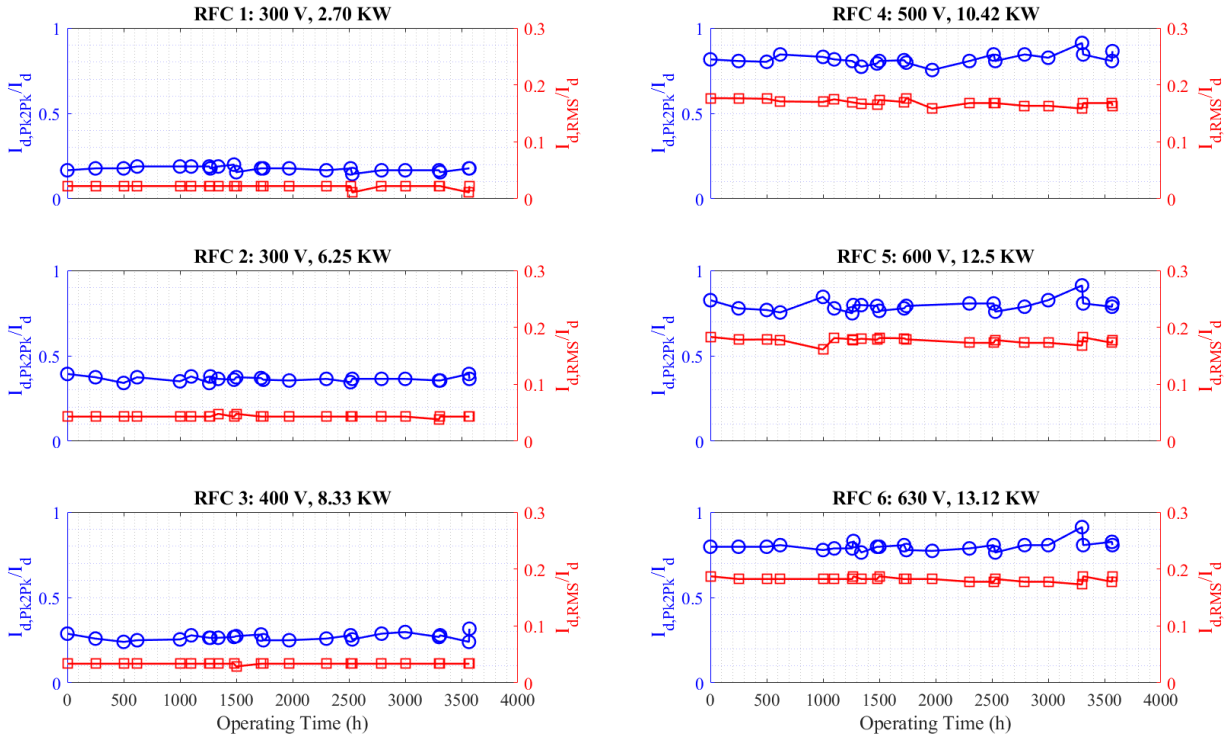

Figure 8.—TDU-3 discharge current oscillation characteristics as a function of operating time during the LDWT.

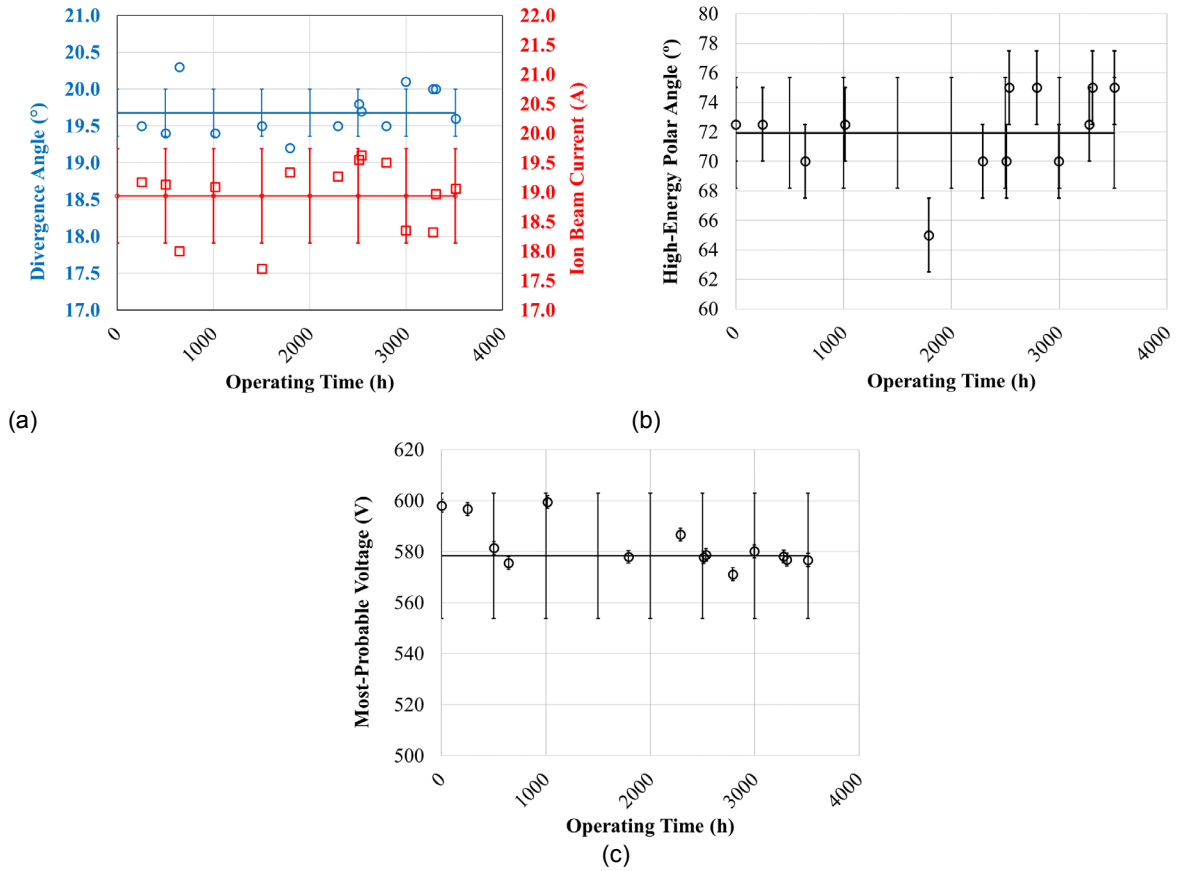

Figure 9.—(a) Charge-weighted divergence angle and ion beam current, (b) maximum high-energy polar angle, and (c) most-probable voltage as a function of operating time for RFC 5 (600 V/12.5 kW) during the TDU-3 LDWT.

TABLE 4.—BACKSPUTTER RATES MEASURED DURING THE TDU-3 LDWT

Location	RFC-5 (600 V/12.5 kW)		RFC-2 (300 V/6.25 kW)	
	Average, μm/kh	Standard deviation, μm/kh	Average, μm/kh	Standard deviation, μm/kh
Outer North	1.56	0.22	----	----
Inner North	1.24	0.28	1.14	0.13
South	1.67	0.12	1.40	0.17

The most-probable voltage found from the centerline RPA trace is shown as a function of operating time Figure 9(c). These values have been corrected for the plasma potential measured by the Langmuir probe. The mean value of the LDWT was found to be 578.4 V, with a standard deviation of 18.3 V (3.2 percent). Overall, all plume measurements are consistent with values obtained during previous TDU performance and wear tests (Refs. 9, 15, 16, and 34). Furthermore, the lack of variation in these values as a function of operating matches the performance and stability data discussed in Sections 4.2 and 4.3, respectively.

4.5 Backsputter

Facility backsputter rates measured during the TDU-3 LDWT are shown in Table 4 for operation at RFC-5 (Segments I and V) and RFC-2 (Segments II-IV). The shown rates were calculated from QCM thickness data sampled every 16 min to reduce noise. Throughout the LDWT, the facility backsputter rate was at all times less than 2 μm/kh and no significant variation in rates was observed with operating time. As shown in Table 4, operation at 300 V resulted in a reduction in facility backsputter rates of approximately 10 to 15 percent relative to operation at 600 V. Overall, these measurements are consistent with previous wear tests, which have observed an average facility backsputter rate of approximately 1.2 μm/kh (Refs. 3 and 30).

4.6 Wear

This section presents an overview of the erosion results obtained only during Segments V-VI of the LDWT. Wear results from Segments I-IV are detailed in Reference 7 while the impact of facility pressure on component erosion is discussed in Reference 35.

4.6.1 Erosion of Carbon-Carbon IFPC

The average erosion rate of the C-C IFPC used during Segment V of the TDU-3 LDWT is shown in Figure 10 along with comparable results acquired with graphite covers during the TDU-1 wear test and Segment I of the LDWT. In Figure 10, a normalized radius of 0 corresponds to the edge of the IFPC closest to the cathode whereas a radius of 1 corresponds to the edge closest to the discharge channel. The truncation of the LDWT data near the inner IFPC edge is due to the fact that the employed masks only covered approximately 95 percent of the IFPC.

Overall, the erosion rates of the C-C IFPC are azimuthally symmetric and match those obtained with graphite pole covers to within the experimental uncertainty. The larger uncertainty associated with the C-C IFPC measurements is primarily due to the woven construction of the C-C composite. This weave results in increased surface roughness and the presence of surface features (e.g., gaps) equal in dimension to the steps introduced by erosion that are not present in the polished graphite covers. Despite these changes, the measurements indicate that the average erosion rates of the C-C IFPC match those of graphite pole covers.

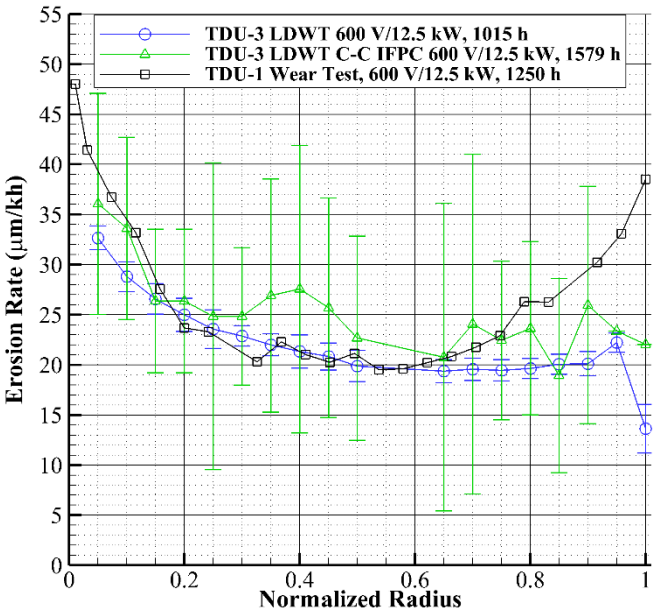

Figure 10.—IFPC erosion rates measured using a C-C IFPC during Segment V of the TDU-3 LDWT.

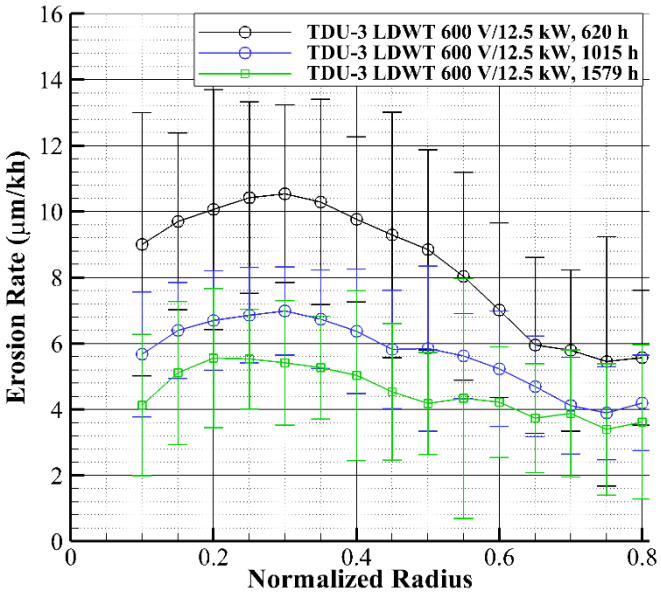

Figure 11.—OFPC erosion rates measured at RFC 5 during the LDWT.

4.6.2 Impact of Polishing

Figure 11 shows the OFPC erosion rates measured during the LDWT as a function of normalized OFPC radius. In Figure 11, a normalized radius of 0 corresponds to the edge of the OFPC closest to the discharge channel whereas a radius of 1 corresponds to the outer edge of the thruster. The truncation of the data near the inner edge is due to the fact that the employed masks do not cover the entire width of the OFPC. Near the outer edge, the mask fastener interfered with the unexposed reference surface, thus precluding data analysis in this region.

Consistent with IFPC measurements presented in previous work, the mean OFPC erosion rates measured at RFC 5 show an apparent decrease with operating time (Refs. 3 and 7). Specifically, the radially-averaged erosion rates decreased by approximately 46 percent between the measurements taken after 600 h and 1579 hours of operation. However, unlike with the IFPC, this decrease is within the uncertainty of the measurement.

Previous work has suggested that this observed decrease in erosion rates over time is actually caused by changes in pole cover surface finish during operation (Ref. 7). Specifically, although polished pre-test, the graphite pole covers have been observed to roughen after plasma exposure. Once roughened, the results in Figure 11, suggest that the erosion rates of the OFPC decrease.

As discussed in Section 3.5.2, masks were placed over both polished and unpolished sections of the OFPC during Segments V and VI of the LDWT in order to assess this hypothesized link between surface finish and erosion rates. For both segments, resolvable net erosion was measured in the regions of the OFPC that were polished pre-test, but no measurable erosion was detected on the unpolished sections of the OFPC. This provides additional evidence supporting the claim that the observed erosion rate time dependence is actually a surface roughness dependence introduced by the pre-test polishing of the pole covers.

This finding could also provide insight into the SDWT results that showed higher erosion rates at 600 V relative to 300 V for operation in VF-6. As noted in Williams et al. (Ref. 4), the 300 V segment of the SDWT performed in VF-6 employed an IFPC that had previously been used. Since this IFPC was not re-polished prior to the start of the 300 V segment, it began the segment roughened, and, therefore, could have exhibited lower erosion rates than would have been measured on a polished IFPC. Thus, the inverted IFPC erosion trend with discharge voltage observed in VF-6 could simply be due to an inconsistency in pole cover finish.

4.6.3 Azimuthal Variations in Keeper Erosion

Two features of note were observed during the keeper wear assessment performed after Segment VI. First, net deposition with a thickness of approximately 1 μm was observed around the keeper orifice. This deposition is shown by the dark ring surrounding the orifice in Figure 12(a) and the rough peaks in the 3D surface scan of the near-orifice region in Figure 12(b). This is quite different from the net erosion observed at all other radii, but it does match observations made during the TDU-1 wear test.

A region of net deposition was also observed on one side of the radial tab that protruded inwards from the keeper mask. This deposition is shown by the dark triangular region near the unexposed keeper region at the 3 o'clock position in Figure 12(a). Evidence of deposition is also visible in the azimuthal profile extracted from this region and shown in Figure 12(c). Specifically, the hill adjacent to the leftmost masked region represents the net deposition observed during Segment V of the LDWT. The two heights visible in the masked region of the profile in Figure 12(c) were caused by the rotation of the keeper mask between Segments V and VI. Specifically, the lower region corresponds to the keeper region masked for Segment V and exposed for Segment VI, whereas the higher region was masked for both segments. This height change obfuscates the measurement of the deposition that occurred during Segment VI, even though a second dark region is visible adjacent to the masked region in Figure 12(a).

It is important to note that deposition was only visible on one side of the keeper mask. One possibility is that this was due to azimuthal variation in the process driving keeper erosion. Further evidence of this is shown in Figure 13, which depicts a sample keeper profile obtained at the end of Segment I of the LDWT. Although a clearly defined step between the masked and unmasked keeper regions is visible to the right of the masked region, almost no step is detectible on the left side of the masked region. This is different from profiles acquired on the IFPC, which have nearly identical steps on both sides of the mask. However, it does match the trends observed during the SDWT (Ref. 4).

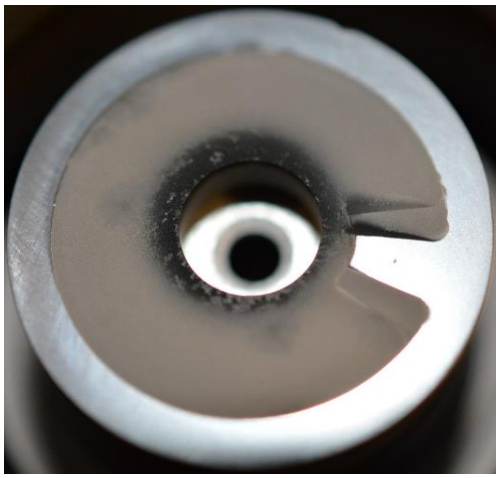

(a)

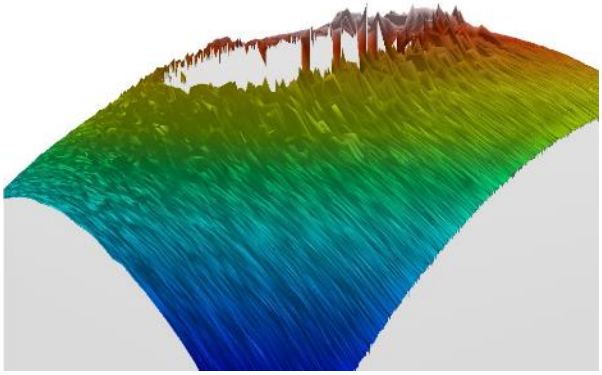

(b)

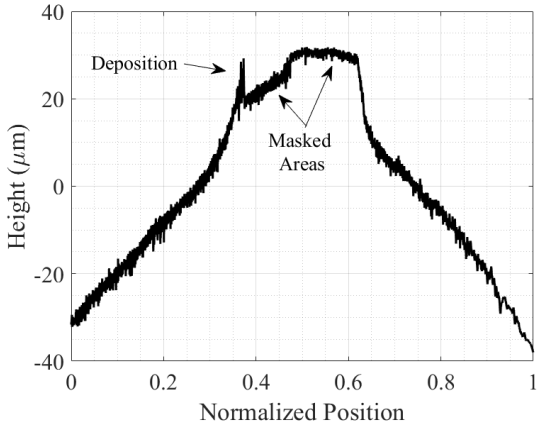

(c)

Figure 12.—A (a) photograph, (b) 3D surface scan, and (c) profile of deposition observed on the keeper after Segment VI of the LDWT.

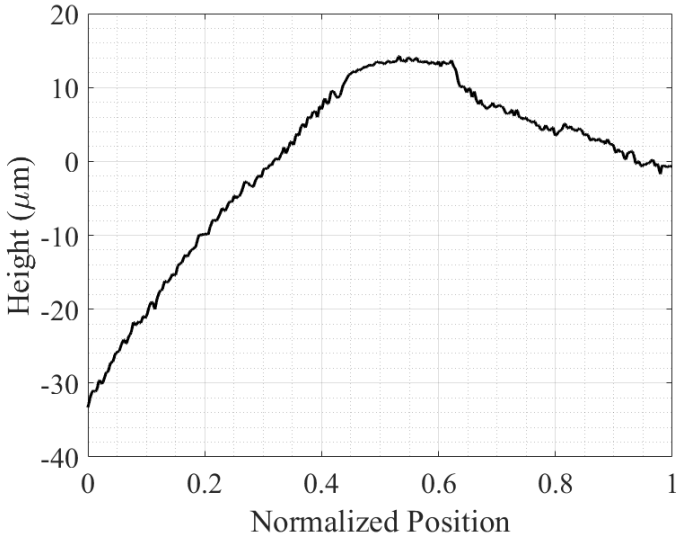

Figure 13.—Sample keeper profile from Segment I of the LDWT.

Another possibility is that the apparent azimuthal variation is an artifact introduced by the orientation of the mask. As shown in Figure 5(a), the radial tab was placed at approximately the 4 o'clock location during Segments V and VI of the LDWT. The side of the tab on which net deposition was observed was therefore approximately horizontal during these segments and faced the ceiling of the facility. Since the top of the facility contains numerous backsputter sources (e.g., pumps, carbon paneling, etc.), the observed net deposition could also be due to a flux of carbon from these sources with a preferential downward angle. However, the keeper mask was oriented with the tab at the 12 o'clock location during Segment I. Thus, although it is a plausible explanation for the net deposition observed during Segments V-VI, this preferential downward flux of carbon cannot explain the azimuthal variation shown in Figure 13. Taken together, this suggests that the azimuthal velocity component of eroding ions is important for understanding HERMeS cathode keeper wear.

5.0 Conclusions

This work presented a summary and overview of the results acquired during the TDU-3 LDWT with a primary focus on the final two test segments. Periodic performance and plume characterizations performed at a set of six fixed reference firing conditions indicated that TDU-3 performance, stability, and plume properties varied by less than the measurement uncertainty throughout the test as well as when compared to results acquired during previous TDU performance and wear characterizations. Facility backsputter was observed to always be less than 2 μm/kh, with lower rates measured for operation at 300 V/6.25 kW relative to 600 V/12.5 kW.

Average erosion rates of a carbon-carbon composite inner front pole cover were found to be azimuthally symmetric and match those obtained with graphite pole covers to within the experimental uncertainty. Consistent with previous TDU wear tests, OFPC erosion rates were shown to decrease with operating time. Observations of lower erosion rates for unpolished sections of the OFPC provide strong evidence that this might be caused by the roughening of the pole covers during operation, rather than a drift in the near-field plasma properties or eroding ion trajectories. Regions of net deposition were observed near the keeper orifice and on one side of the keeper mask. This matches results obtained during previous TDU wear tests and suggests the presence of an azimuthal variation in the process driving keeper erosion.

Overall, the TDU-3 LDWT successfully served as a pathfinder for the planned life and qualification testing of AEPS hardware. The HERMeS thruster design was shown to satisfy all AEPS performance requirements over more than 3500 h of operation while exhibiting component lifetime margins of greater than 40 percent at the nominal 600 V/12.5 kW operating condition. NASA-provided diagnostics were successfully demonstrated and provided consistent performance over the entire wear test while facility procedures were developed and successfully tested for all planned AEPS test operations. The opportunity afforded by the LDWT to develop this experience with operating long duration testing of high-power Hall thrusters will significantly lower the risks for all future extended duration tests and likely prove invaluable in the preparation of AEPS for integration with the lunar Gateway.

References

1. Congress, National Aeronautics and Space Administration Transition Authorization Act of 2017. 2017.
2. Smith, B.K., Nazario, M.L., and Cunningham, C.C., "Solar Electric Propulsion Vehicle Demonstration to Support Future Space Exploration Missions," Cleveland, OH, 2012.

3. Williams, G., Gilland, J.H., Peterson, P.Y., Kamhawi, H., Huang, W., Swiatek, M., Joppeck, C., et al., "2000-hour Wear Testing of the HERMeS Thruster," 52nd AIAA/SAE/ASEE Joint Propulsion Conference, American Institute of Aeronautics and Astronautics, AIAA Paper 2016-5025, Reston, VA, 2016, doi:10.2514/6.2016-5025.
4. Williams, G.J., Kamhawi, H., Choi, M., Haag, T., Huang, W., Herman, D.A., Gilland, J.H., et al., "Wear Trends of the HERMeS Thruster as a Function of Throttle Point," 35th International Electric Propulsion Conference, IEPC Paper 2017-207, Fairview Park, OH, 2017.
5. Benavides, G.F., Mackey, J., Ahern, D.M., and Thomas, R., "Diagnostic for Verifying the Thrust Vector Requirement of the AEPS Hall-Effect Thruster and Comparison to the NEXT-C Thrust Vector Diagnostic," presented at the 2018 Joint Propulsion Conference, Reston, VA, American Institute of Aeronautics and Astronautics, AIAA Paper 2018-4514, Reston, VA, 2018.
6. Ahern, D.M., Frieman, J.D., Williams, G.J., Mackey, J., Haag, T.W., Huang, W., Kamhawi, H., et al., "In-situ Diagnostic for Assessing Hall Thruster Wear," 2018 Joint Propulsion Conference, American Institute of Aeronautics and Astronautics, AIAA Paper 2018-4721, Reston, VA, 2018.
7. Frieman, J.D., Kamhawi, H., Williams, G.J., Huang, W., Herman, D.A., Peterson, P.Y., Gilland, J.H., et al., "Long Duration Wear Test of the NASA HERMeS Hall Thruster," 2018 Joint Propulsion Conference, American Institute of Aeronautics and Astronautics, AIAA Paper 2018-4645, Reston, VA, 2018.
8. Hofer, R.R., Polk, J.E., Sekerak, M.J., Mikellides, I.G., Kamhawi, H., Sarver-Verhey, T.R., Herman, D.A., et al., "The 12.5 kW Hall Effect Rocket with Magnetic Shielding (HERMeS) for the Asteroid Redirect Robotic Mission," 52nd AIAA/SAE/ASEE Joint Propulsion Conference, American Institute of Aeronautics and Astronautics, AIAA Paper 2016-4825, Reston, VA, 2016, doi:10.2514/6.2016-4825.
9. Kamhawi, H., Huang, W., Gilland, J., Haag, T., Mackey, J., Yim, J., Pinero, L., et al., "Performance, Stability, and Plume Characterization of the HERMeS Thruster with Boron Nitride Silica Composite Discharge Channel," 35th International Electric Propulsion Conference, Electric Rocket Propulsion Society, IEPC Paper 2017-392, Fairview Park, OH, 2017.
10. Mikellides, I.G., Katz, I., Hofer, R.R., Goebel, D.M., de Grys, K., and Mathers, A., "Magnetic shielding of the channel walls in a Hall plasma accelerator," Physics of Plasmas, 2011, p. 033501, doi: 10.1063/1.3551583.
11. Mikellides, I.G., Katz, I., Hofer, R.R., and Goebel, D.M., "Magnetic Shielding of a Laboratory Hall Thruster. I. Theory and Validation," Journal of Applied Physics, 2014, p. 043303, doi: 10.1063/1.4862313.
12. Mikellides, I., Katz, I., Hofer, R., Goebel, D., de Grys, K., and Mathers, A., "Magnetic Shielding of the Acceleration Channel Walls in a Long-Life Hall Thruster," 46th AIAA/ASME/SAE/ASEE Joint Propulsion Conference & Exhibit, American Institute of Aeronautics and Astronautics, AIAA Paper 2010-6942, Reston, VA, 2010, doi:10.2514/6.2010-6942.
13. Snyder, J.S., Baldwin, J., Frieman, J.D., Walker, M.L.R., Hicks, N.S., Polzin, K.A., and Singleton, J.T., "Recommended practice for flow control and measurement in electric propulsion testing," Journal of Propulsion and Power, 2017, doi: 10.2514/1.B35644.
14. Piñero, L.R., "The Impact of Harness Impedance on Hall Thruster Discharge Oscillations," 35th International Electric Propulsion Conference, Electric Rocket Propulsion Society, IEPC Paper 2017-023, Fairview Park, OH, 2017.
15. Kamhawi, H., Huang, W., Haag, T., Yim, J., Herman, D., Peterson, P.Y., Williams, G., et al., "Performance, Facility Pressure Effects, and Stability Characterization Tests of NASA's Hall Effect Rocket with Magnetic Shielding Thruster," 52nd AIAA/SAE/ASEE Joint Propulsion Conference, American Institute of Aeronautics and Astronautics, Reston, VA, 2016, doi:10.2514/6.2016-4826.

16. Huang, W., Kamhawi, H., and Haag, T., "Facility Effect Characterization Test of NASA's HERMeS Hall Thruster," 52nd AIAA/SAE/ASEE Joint Propulsion Conference, American Institute of Aeronautics and Astronautics, AIAA Paper 2016-4828, Reston, VA, 2016, doi:10.2514/6.2016-4828.
17. Peterson, P.Y., Kamhawi, H., Huang, W., Williams, G., Gilland, J.H., Yim, J., Hofer, R.R., et al., "NASA's HERMeS Hall Thruster Electrical Configuration Characterization," 52nd AIAA/SAE/ ASEE Joint Propulsion Conference, American Institute of Aeronautics and Astronautics, AIAA Paper 2016-5027, Reston, VA, 2016, doi:10.2514/6.2016-5027.
18. Frieman, J.D., King, S.T., Walker, M.L.R., Khayms, V., and King, D., "Role of a conducting vacuum chamber in the hall effect thruster electrical circuit," Journal of Propulsion and Power, 2014, pp. 1471–1479, doi: 10.2514/1.B35308.
19. Lobo, M.J., "Electric Propulsion Laboratory | NASA Glenn Research Center," 2017.
20. Yim, J. and Burt, J.M., "Characterization of Vacuum Facility Background Gas Through Simulation and Considerations for Electric Propulsion Ground Testing," 51st AIAA/SAE/ASEE Joint Propulsion Conference, American Institute of Aeronautics and Astronautics, AIAA Paper 2015-3825, Reston, VA, 2015, doi:10.2514/6.2015-3825.
21. Yim, J.T., Herman, D.A., and Burt, J.M., "Modeling Analysis for NASA GRC Vacuum Facility 5 Upgrade," NASA Glenn Research Center, Cleveland, OH, NASA/TM—2013-216496, 2013.
22. Dankanich, J.W., Walker, M., Swiatek, M.W., and Yim, J.T., "Recommended Practice for Pressure Measurement and Calculation of Effective Pumping Speed in Electric Propulsion Testing," Journal of Propulsion and Power, 2017, pp. 668–680, doi: 10.2514/1.B35478.
23. "Standard Practice for Ionization Gage Application to Space Simulators," ASTM International, West Conshohocken, PA, E296-70, 2015.
24. Frieman, J.D., Liu, T.M., and Walker, M.L.R., "Background flow model of hall thruster neutral ingestion," Journal of Propulsion and Power, 2017, doi: 10.2514/1.B36269.
25. Peterson, P.Y., Kamhawi, H., Huang, W., Yim, J., Haag, T., Mackey, J., Mcvetta, M., et al., "Reconfiguration of NASA GRC's Vacuum Facility 6 for Testing of Advanced Electric Propulsion System (AEPS) Hardware," 35th International Electric Propulsion Conference, Electric Rocket Propulsion Society, IEPC Paper 2017-028, Fairview Park, OH, 2017.
26. Xu, K.G. and Walker, M.L.R., "High-power, Null-type, Inverted Pendulum Thrust Stand," Review of Scientific Instruments, 2009, pp. 55103–55103, doi: 10.1063/1.3125626.
27. Haag, T.W., "Thrust Stand for High-power Electric Propulsion Devices," Review of Scientific Instruments, 1991, pp. 1186–1191, doi: 10.1063/1.1141998.
28. Pancotti, A., Haag, T., King, S., and Walker, M., "Recommended Practices in Thrust Measurements," 33rd International Electric Propulsion Conference, Electric Rocket Propulsion Society, IEPC Paper 2013-440, Fairview Park, OH, 2013.
29. Mackey, J., Haag, T.W., Kamhawi, H., Hall, S.J., and Peterson, P.Y., "Uncertainty in Inverted Pendulum Thrust Measurements," 54th AIAA/SAE/ASEE Joint Propulsion Conference, American Institute of Aeronautics and Astronautics, AAA Paper 2018-4516, Reston, VA, 2018.
30. Gilland, J.H., Williams, G., Burt, J.M., and Yim, J., "Carbon Back Sputter Modeling for Hall Thruster Testing," 52nd AIAA/SAE/ASEE Joint Propulsion Conference, American Institute of Aeronautics and Astronautics, AIAA Paper 2016-4941, Reston, VA, 2016, doi:10.2514/6.2016-4941.
31. Standardization, I.O. for, "ISO 5436-1:2000 Geometrical Product Specifications (GPS) - Surface texture: Profile method; Measurement standards - Part 1: Material measures," 2003.
32. Mackey, J., Frieman, J.D., Ahern, D.M., and Gilland, J.H., "Uncertainty in Electric Propulsion Erosion Measurements," 2019 Joint Propulsion Conference, 2019.

33. Fisher, J., Wilson, A., and Werthman, L., "The Qualification of a 4.5 kW Hall Thruster Propulsion Subsystem," 39th AIAA/ASME/SAE/ASEE Joint Propulsion Conference and Exhibit, American Institute of Aeronautics and Astronautics, AIAA Paper 2003-4551, Reston, VA, 2003, doi:10.2514/6.2003-4551.
34. Huang, W., Williams, G.J., Peterson, P.Y., Kamhawi, H., Gilland, J.H., and Herman, D.A., "Plasma Plume Characterization of the HERMeS during a 1722-hr Wear Test Campaign," 35th International Electric Propulsion Conference, Electric Rocket Propulsion Society, IEPC Paper 2017-307, Fairview Park, OH, 2017.
35. Frieman, J.D., Kamhawi, H., Peterson, P.Y., Herman, D.A., Gilland, J.H., and Hofer, R.R., "Impact of Facility Pressure on the Wear of the NASA HERMeS Hall Thruster," 36th International Electric Propulsion Conference, Electric Rocket Propulsion Society, Fairview Park, OH, 2019.